

1 **Flat slab-induced hydration weakening and destruction**  
2 **of the North China Craton**

3 **Jyotirmoy Paul, Arne Spang, Andrea Piccolo**

4 Bayerisches Geoinstitut, Universität Bayreuth, 95447 Bayreuth, Germany

5 **Key Points:**

- 6 • Investigation of North China Craton (NCC) destruction with thermomechanical  
7 numerical models.  
8 • Flat slab-induced hydration can sufficiently weaken eastern part of the North China  
9 Craton (NCC).  
10 • Craton is destroyed if its density is higher than the underlying mantle and its vis-  
11 cosity is lower than  $10^{22}$  Pa s.

---

Corresponding author: Jyotirmoy Paul, [jyotirmoy.paul@uni-bayreuth.de](mailto:jyotirmoy.paul@uni-bayreuth.de)

**Abstract**

In this study, we develop two dimensional (2-D) box models to identify the most viable reasons for the destruction of the North China Craton (NCC). We examine the role of flat slab-induced hydration, high-density lower crust, and weak mid-lithospheric discontinuity in our models. Results indicate that flat slab-induced hydration weakening of the eastern part of the NCC can lead to rapid craton destruction if hydration weakening rates are sufficiently fast. This accelerated hydration rate may be attributed to the extensive carbonatite magmatism within the eastern part of the NCC, facilitating a faster pathway for water diffusion throughout the craton. Craton destruction is contingent upon the craton's density exceeding the surrounding mantle density, and its viscosity decreasing below  $10^{22}$  Pa s. We observe that the presence of a dense lower crust or a weak mid-lithospheric discontinuity fail to destroy the NCC unless it is weakened.

**Plain Language Summary**

Cratons, constituting the oldest part of Earth's lithosphere, often exceed 3 billion years in age. Despite continuous recycling due to plate-tectonics on Earth, cratons maintain tectonic stability owing to their viscosity, density, and thickness. Nevertheless, certain geological activities can lead to the partial or complete destruction of cratons. A prime example is the North China Craton (NCC), where the eastern half has undergone extensive thinning. The mechanism behind the NCC's destruction has been a subject of debate for over the last two decades. In this study, we develop numerical models to investigate the most viable geodynamic scenario for the destruction of the NCC. We find hydration weakening, induced by fluids from the subducting slab, is the key control for craton destruction. Geological evidence indicates the flattening of the subducting slab during the Jurassic period. The presence of a flat slab likely facilitated partial hydration of the eastern half of the craton, while the western half remained intact. Subsequently, the weakened eastern segment could have been destroyed due to underlying mantle flow if the craton possessed a density exceeding underlying mantle and a viscosity lower than  $10^{22}$  Pa s.

**1 Introduction**

Destruction of the North China Craton (NCC) (F.-Y. Wu et al., 2019; J. T.-J. Wu et al., 2022; Y.-F. Zheng et al., 2013; Zhu et al., 2012) challenges the notion of immortal cratons in geological history. Geophysical evidence, including the global lithospheric thickness model (Conrad & Lithgow-Bertelloni, 2006) (Fig. 1 A), slow seismic velocity anomalies in tomography models (Ritsema et al., 2004)(Fig. 1 A), and geochemical observations from xenolith studies (Menzies et al., 1993; Xu, 2001; Yang et al., 2008; J. Zheng et al., 2005; Y. Zheng et al., 2018; Zhu et al., 2012), firmly establish that the eastern part of the North China Craton is thinner than its western counterpart. Prior  $\sim 200$  Ma (early Jurassic period), the entire craton existed with a passive margin boundary and a normal cratonic thickness of approximately 200 km (Z. Wang & Kusky, 2019, c.f.). After 200 Ma, the onset of paleo-Pacific subduction along the eastern margin of the NCC reactivated the craton margin (Tang et al., 2018). In the early Cretaceous period ( $\sim 130$  - 100 Ma), the eastern part of the craton thickness was reduced to around 100 km (Zhu et al., 2012; F.-Y. Wu et al., 2019; J. T.-J. Wu et al., 2022; J. Zheng et al., 2005; Y. Zheng et al., 2018; J. Liu et al., 2019). Although there is consensus regarding the extensive thinning of the NCC, the mechanism behind it remains a subject of debate.

Previous studies proposed a range of possible mechanisms that could destroy the eastern part of the NCC. The onset of paleo-Pacific subduction at the eastern margin of the NCC has been considered as one of the most likely reasons for craton destruction (Xu, 2001; J. Zheng et al., 2005). The nature of the subduction zone remained disputed

61 for a long time until recently, when several studies proposed the existence of a flat slab  
62 in this region. F.-Y. Wu et al. (2019) showed an age reversal of igneous rocks along an  
63 east-west transect from the paleo-subduction zone to the middle of the craton (Fig. 1  
64 B). Many of these igneous activities are associated with carbonatite intrusions, partic-  
65 ularly from the eastern part of the NCC (Chen et al., 2016, 2017; X. Wang et al., 2022).  
66 During the late Triassic and Jurassic periods, magmatic activities moved towards the  
67 continental interior, and in the Cretaceous period, magmatism migrated towards the sea  
68 (Fig. 1 C). This reversal is interpreted as the onset of westward flat subduction of the  
69 Paleo-Pacific slab around 200 Ma, followed by slab rollback at approximately 160 - 140  
70 Ma (Y. Zheng et al., 2018; J. Liu et al., 2019; F.-Y. Wu et al., 2019; J. T.-J. Wu et al.,  
71 2022) (Fig. 1 C). The presence of a flat slab could have hydrated the eastern part of the  
72 craton (Fig. 1 C, hatched region) (F.-Y. Wu et al., 2019; J. T.-J. Wu et al., 2022; Y. Zheng  
73 et al., 2018), while the western block remained dry (Xia, Hao, et al., 2013). Xia, Liu, et  
74 al. (2013) studied the clinopyroxene samples of early Cretaceous basalts from the Feix-  
75 ian region (Fig. 1 A) and found high water content within them. They estimated that  
76 such high water content in clinopyroxene samples is possible only if the cratonic man-  
77 tle contained at least 1000 ppm water before  $\sim 120$  Ma. Such high water content can  
78 change the 'dry' olivine rheology to 'wet' olivine (Hirth & Kohlstedt, 2003; Mei & Kohlst-  
79 edt, 2000; Xia, Liu, et al., 2013), significantly reducing the overall viscosity of the litho-  
80 spheric mantle. Weaker cratons potentially form lithospheric drips depending on their  
81 'available buoyancy' (Conrad & Molnar, 1999), and those drips are removed gradually.  
82 Y. Zheng et al. (2018) attributed the NCC destruction to such a bottom-to-top process.

83 There are other mechanisms that could also have destroyed the NCC. Due to high  
84 pressure and temperature, dense eclogites are formed within the thick lower crust. This  
85 dense layer initiates a gravitational instability which can delaminate the crust, and even-  
86 tually destroy the cratonic lithosphere by a process called foundering (Gao et al., 2004).  
87 Other studies have suggested the presence of a weak mid-lithospheric discontinuity (MLD)  
88 as another potential reason for craton destruction (Liao & Gerya, 2014; L. Liu et al., 2019;  
89 Shi et al., 2020; Z. Wang & Kusky, 2019). Unlike the slab-induced process, these two  
90 destruction mechanisms are top-to-bottom processes, where craton destruction initiates  
91 at the top margin (Y. Zheng et al., 2018).

92 In this study, we use thermomechanical numerical models to investigate the evo-  
93 lution and destruction of the North China Craton. We investigate several scenarios to  
94 test their mechanical and geodynamical viability. Though our primary focus is to un-  
95 derstand flat slab-induced destruction, we also examine cases in the presence of a dense  
96 lower crustal layer and a weak mid-lithospheric discontinuity. We explore different pa-  
97 rameters, including density, viscosity, and the rate of hydration to support our arguments.  
98 We calibrate the timing of destruction with geologically observed data.

## 99 2 Geodynamic model

100 We develop time-dependent geodynamic models, using the thermomechanical fi-  
101 nite differences code LaMEM (Kaus et al., 2016, details in supplementary text S1) which  
102 is routinely used to model subduction dynamics (Pusok & Stegman, 2020; Riel et al.,  
103 2023). Our 2D model domain consists of a Cartesian box of  $4000 \times 1000$  km (Fig. 2A)  
104 and is built with geomIO (Bauville & Baumann, 2019; Spang, Baumann, & Kaus, 2022).  
105 The continental block comprises a 40 km thick continental crust, followed by a thick con-  
106 tinental lithosphere down to 100 km and a cratonic lithosphere root extending to a depth  
107 of 200 km, with a width of 2000 km (Fig. 2 A). Below the continental lithosphere, the  
108 upper mantle extends to 660 km depth, and the lower mantle to 1000 km. Each layer  
109 is distinguished by a specific rheology given in supplementary table S1 (Hirth & Kohlst-  
110 edt, 2003; Tirel et al., 2008). To simulate the paleo-Pacific subduction zone, we place  
111 a flat slab along the eastern margin of the craton following the approach of F.-Y. Wu  
112 et al. (2019) (Figs. 1 C, 2 A). The flat slab extends to the middle of the craton's width,

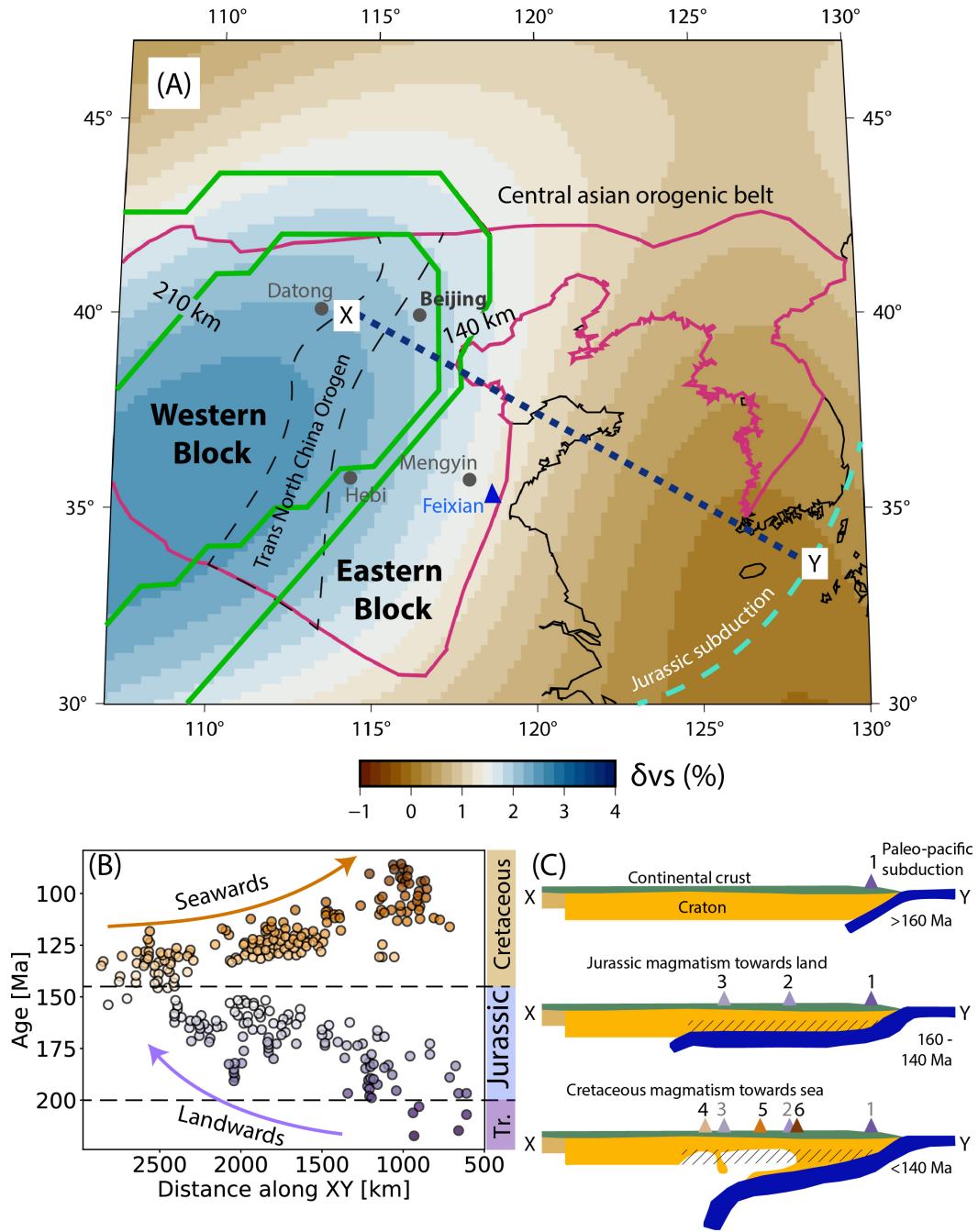


**Figure 1.** (A) Location of the North China Craton (NCC) marked by pink boundary. The western and eastern blocks of the NCC are separated by the trans North China orogen. The background colors in the Figure represent the shear wave velocity anomaly from the S20RTS tomography model (Ritsema et al., 2004), and the green lines are the contours of lithosphere thickness of 210 and 140 km, obtained from the global lithosphere thickness model of Conrad and Lithgow-Bertelloni (2006). Present-day coastlines are in black. Several igneous rocks are dated along the X-Y transect (F.-Y. Wu et al., 2019; J. T.-J. Wu et al., 2022). (B) Age distribution of igneous rocks along X-Y transect extracted and compiled from (Z. Wang & Kusky, 2019; J. T.-J. Wu et al., 2022). (C) Schematic diagram of destruction of North China Craton modified after J. Liu et al. (2019); F.-Y. Wu et al. (2019); J. T.-J. Wu et al. (2022). 1-6 represent progression of magmatic activity with time.

113 hypothetically dividing it into eastern and western part. The mantle flow dynamics are  
 114 driven by the density anomaly of the slab and an additional inflow of 1-2 cm yr<sup>-1</sup> from  
 115 the eastern margin of our model. Additionally, a temperature difference of 1600 K be-  
 116 tween the top and the bottom of the model also contributes to the vigour of mantle flow.  
 117 The upper and lower viscosity cut-offs are 10<sup>18</sup> and 10<sup>25</sup> Pa s. Thermal expansivity ( $\alpha$ ),  
 118 specific heat ( $C_p$ ) and thermal conductivity ( $k$ ) are  $3 \times 10^{-5}$  K<sup>-1</sup>, 1200 J K<sup>-1</sup> kg<sup>-1</sup>,  
 119 and 3.3 W m<sup>-1</sup> K<sup>-1</sup>, respectively.

120 The choice of density of the cratonic block is a key parameter for destruction. It  
 121 is quite challenging to estimate the density of the original craton before the destruction  
 122 started. (Ye et al., 2021) used the in-situ single crystal diffraction method to obtain the  
 123 pressure-temperature-volume distribution of the minerals obtained from the xenoliths  
 124 of the eastern NCC. Further using a third order Birch-Murnaghan equation of state, Ye  
 125 et al. (2021) estimated the density profile of the original craton (Fig. 2 B, black dashed  
 126 line) at  $\sim 200$  Ma. We choose different density profiles ( $\rho_i$ ) for cratons by varying their  
 127 reference density ( $\rho_i^0$ ) between 3400, 3300, and 3200 kg m<sup>-3</sup> at 20 °C, respectively. The  
 128 actual densities are calculated as  $\rho_i = \rho_i^0(1 - \alpha\delta T)$ , where  $\alpha$  and  $\delta T$  are the thermal ex-  
 129 pansivity ( $3 \times 10^{-5}$  K<sup>-1</sup>) and deviation of temperature from 20 °C. While the estimated  
 130 density by Ye et al. (2021) falls within the range of 3280 to 3300 kg m<sup>-3</sup> (Fig 2 B, black  
 131 dashed line), our models show similar densities to the estimated value, ranging between  
 132 3180 and 3300 kg m<sup>-3</sup> (Fig. 2 B). Each density model is tested with three different weak-  
 133 ening rates (see next paragraph) to have 9 models (models M1-M9, Table S2). We also  
 134 test a another 9 models including high density lower crust and weak mid-lithospheric dis-  
 135 continuity (models M10 - M18, Fig. 2 C, Table S2). The dense lower crust is added at  
 136 30-70 km depth in models M13- M15 and the mid-lithospheric discontinuity is added at  
 137 60-100 km depth in models M16-M18.

138 To approximate gradual hydration-induced weakening in the eastern part of the  
 139 craton, we divide the cratonic lithosphere into six thin layers (Fig. 2 A). Each layer grad-  
 140 ually transitions (Spang, Burton, et al., 2022) from a dry olivine rheology to a wet olivine  
 141 rheology from bottom to top (Supplementary Table 1). This transition is deemed real-  
 142 istic based on the estimated high water content within the NCC (Xia, Liu, et al., 2013).  
 143 Dry olivine rheology makes the craton highly viscous, with a viscosity exceeding 10<sup>24</sup> Pa  
 144 s, while wet olivine rheology results in a viscosity of less than 10<sup>22</sup> Pa s. However, de-  
 145 termining the exact timing of hydration of the cratonic lithosphere poses a significant  
 146 challenge. While some studies (J. Liu et al., 2019) have estimated the timing of slab dy-  
 147 namics and craton destruction, there is no consensus on the duration required for cra-  
 148 ton hydration. Experimental studies have suggested a wide range of hydrogen diffusiv-  
 149 ities, ranging from 10<sup>-11</sup> to 10<sup>-4</sup> m<sup>2</sup> s<sup>-1</sup> (Demouchy et al., 2007; Demouchy, 2010; Kohlst-  
 150 edt & Mackwell, 1998). Demouchy (2010) predicted a diffusivity of  $5.11 \times 10^{-6}$  m<sup>2</sup> s<sup>-1</sup>  
 151 to be a reasonable estimate for upper mantle conditions at 1200 °C. At this rate, wa-  
 152 ter can diffuse through 100 km in approximately 60 Myr (Fig. 2 D). Several studies have  
 153 suggested that the rate of hydration could be accelerated if it is controlled by carbon-  
 154 atite melts (Hammouda & Laporte, 2000; X. Wang et al., 2022), which are abundant in  
 155 the NCC (Chen et al., 2016, 2017; X. Wang et al., 2022). Additionally, some recent hy-  
 156 potheses propose that water infiltration along the slab gap may have also influenced the  
 157 rate of hydration weakening within the NCC (Z. Wang et al., 2023). Based on various  
 158 calculations, we assume three different weakening rates, R1, R2, and R3 (Fig. 2 D), for  
 159 the hydration of the eastern block of the NCC. R3 weakens each thin layer after 9 Myr,  
 160 weakening the 100 km thick lithosphere within 54 Myr, closely matching the water dif-  
 161 fusion timescale estimated by Demouchy (2010). R1 represents the fastest weakening rate,  
 162 which can hydrate each thin layer in a time interval of 2.5 Myr, weakening the cratonic  
 163 block within 15 Myr. This faster hydration rate still falls within the estimated range of  
 164 water diffusion within the mantle (Fig. 2 D). To further assess the effect of weakening  
 165 rates in our models, we choose another intermediate case R2, which can weaken the cra-

166 ton within 24 Myr. In the following sections, we analyze the results from 18 different mod-  
 167 els and discuss the factors contributing to craton destruction.

### 168 3 Results

#### 169 3.1 Flat slab-induced hydration weakening and craton destruction

170 Amongst 18 models, we first discuss about model M2 that utilizes a fast weaken-  
 171 ing rate (R1, Fig. 2 D) and a reference density of  $3300 \text{ kg m}^{-3}$ . With this combination,  
 172 the craton initially possesses a viscosity of the order of  $10^{24} \text{ Pa s}$  (Fig. 3) and a density  
 173 between  $3200\text{--}3250 \text{ kg m}^{-3}$  (Fig. 2 B). The chosen density and viscosity maintain the  
 174 craton in equilibrium above the mantle. The slab's density is slightly higher than that  
 175 of the surrounding mantle, triggering subduction in the model. As the slab moves down-  
 176 ward, it induces convection in the mantle, pushing the flow eastwards beneath the cra-  
 177 ton. Concurrently, as the craton gradually weakens from its base, mantle flow begins to  
 178 shear the weakened cratonic material, leading to the formation of lithospheric drips. Some  
 179 weakened sections of the craton sink towards the slab by mantle flow, where they are re-  
 180 cycled into the mantle alongside the subducting slab. By 17 Myr, the cratonic lithosphere  
 181 is completely weakened, and most lithospheric drips detach from the craton's base (Figs.  
 182 3 A, B, video S1). Within 40 Myr, majority cratonic lithosphere is recycled into man-  
 183 tle (Figs. 3 C, D).

184 We calculate the percentage of mantle material replacing cratonic material in the  
 185 eastern block over time (Fig. 4). Initially, there is no mantle material replacing within  
 186 the cratonic block. As cratonic material is removed, the void is replaced by upper man-  
 187 tle material. The increase in mantle material signifies the removal of cratonic material.  
 188 From now on, we will use craton destruction or replacement of mantle material synony-  
 189 mously. Our tracking reveals that approximately 50% of mantle material replaces the  
 190 original craton within just 20 Myr (Fig. 4 A, solid pink line for model M2), indicating  
 191 a swift destruction of the majority of the craton. After the major destruction event, a  
 192 slower process removes up to  $\sim 70\%$  of cratonic material within 40 Myr. The destruc-  
 193 tion further slows down due to the slab stagnating above lower mantle after  $\sim 40$  Myr  
 194 (Figs. 3 C, D).

#### 195 3.2 Effect of density and weakening rates

196 To comprehensively understand the mechanism of craton destruction, we conduct  
 197 additional tests with different density profiles having reference densities  $3400 \text{ kg m}^{-3}$  (M1)  
 198 and  $3200 \text{ kg m}^{-3}$  (M3) (Fig 2 A). Model M1 yields an actual density ranging between  
 199  $3250$  and  $3300 \text{ kg m}^{-3}$  (Fig. 2 A). Here, we observe  $\sim 80\%$  replacement of mantle ma-  
 200 terial within the eastern part of the craton within a time interval of around 20 Myr (Fig.  
 201 4 A, solid blue line). This suggests that a high density craton can experience more rapid  
 202 destruction. Conversely, in model M3 (Table S2), where the craton density is lower than  
 203  $3200 \text{ kg m}^{-3}$ , only 5-10% of the craton has been destroyed (Fig. 4 A, solid cyan line),  
 204 indicating that a craton with a density lower than  $3200 \text{ kg m}^{-3}$  may not undergo de-  
 205 struction even if it is weakened rapidly.

206 We further explore various hydration weakening rates using three sets of different  
 207 density models. For models M1-M3, the fastest weakening rate (R1) is applied, i.e., weak-  
 208 ening 100 km of craton within 15 Myr (Fig. 2 D). The intermediate weakening rate (R2),  
 209 which weakens 100 km craton in 24 Myr, is applied in models M4-M6 (Table S2). Fi-  
 210 nally, the slowest weakening rate (R3), weakening 100 km of craton in 54 Myr, is used  
 211 in models M7-M9 (Table S2). Regardless of the weakening rate, models with craton den-  
 212 sity below  $3200 \text{ kg m}^{-3}$  (models M3, M6, M9) show no significant craton destruction (Fig.  
 213 4 A, cyan lines). The amount of craton destruction is quite similar in the case of the R1  
 214 and R2 weakening rates. Both show rapid destruction of approximately 80% (models M1,

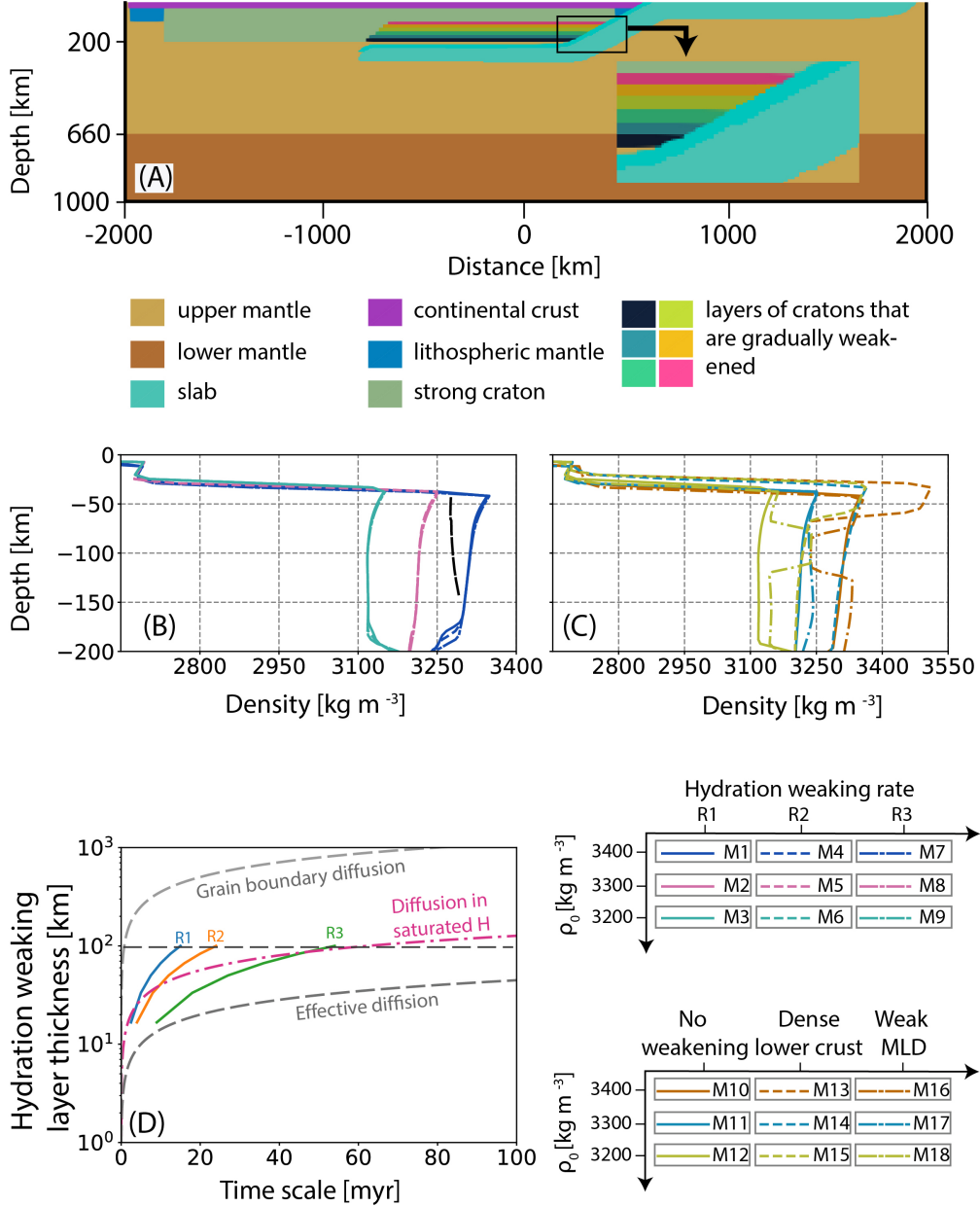


**Figure 2.** A: The geometry used for models M1-M9 is depicted, with each geological unit indicated by a specific color as indexed below. (B, C) The density profiles within the craton obtained from the 18 models is illustrated, with each line representing a specific model. The legend for B, C is provided in the lower right of the Figure. The black dashed line in (B) represents the density estimate of the NCC before destruction (Ye et al., 2021). (D) Hydration weakening rates calculated for different scenarios are presented. The Y-axis shows the thickness of a cratonic lithosphere that can be hydrated, while the X-axis represents the time required to hydrate that thickness of lithosphere. The top and bottom grey dashed lines represent the slowest and fastest weakening rates for hydration weakening calculated from the experimental data provided by Demouchy (2010). The pink dash-dot line represents the hydration weakening rate for upper mantle water diffusion rate in saturated conditions estimated by Demouchy (2010). R1, R2, and R3 denote the three hydration weakening rates utilized for this study.

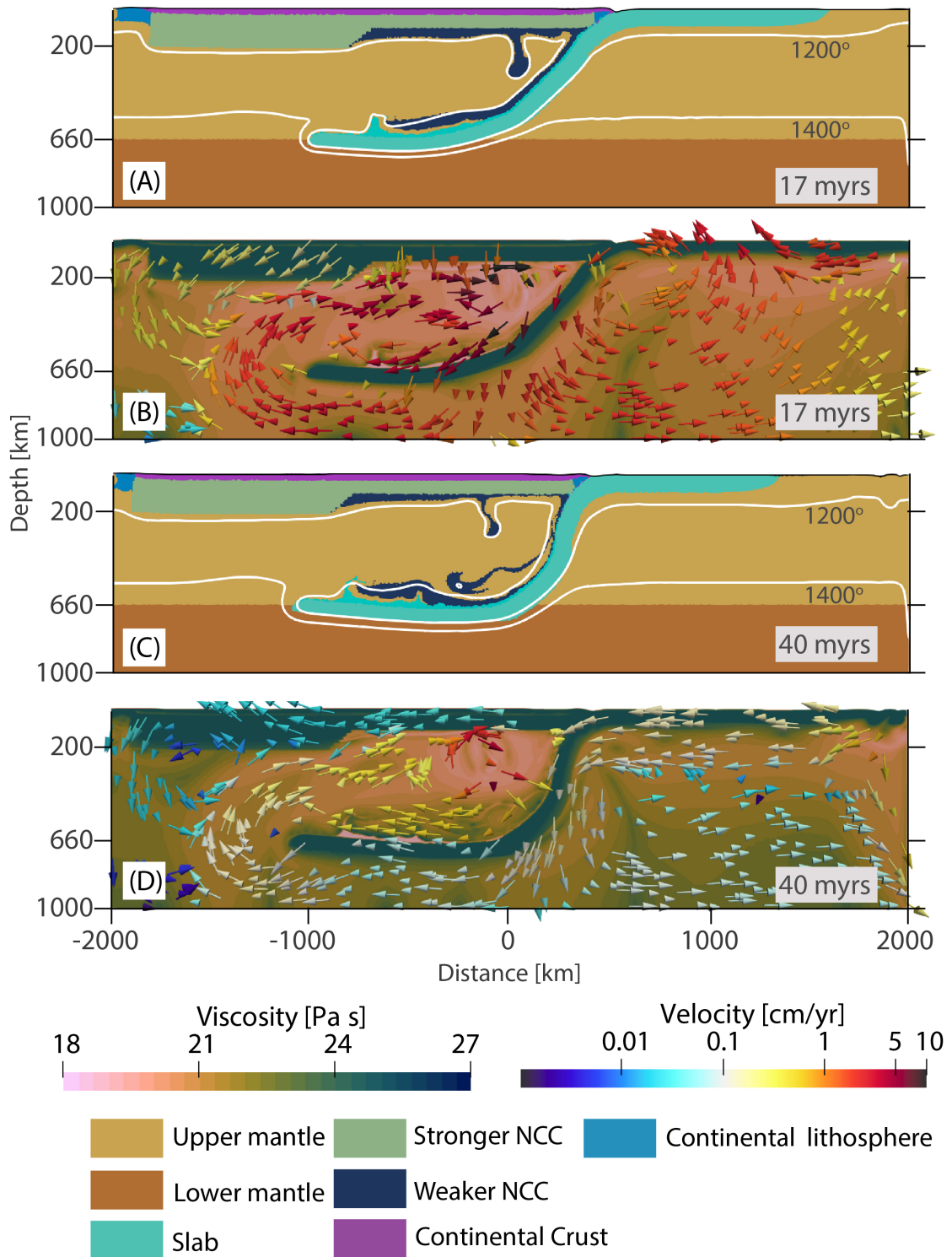


**Figure 3.** Snapshots of the NCC destruction from model M2 after 17 Myr (A-B) and 40 Myrs (C-D) respectively. Background colors in (A, C) represent geological units which are indexed below. Dark blue region indicates the weak craton which is forming lithospheric drips. White lines indicate isotherms of 1200°C and 1400°C. Background colors in (B,D) represent viscosity and the arrows represent velocity.

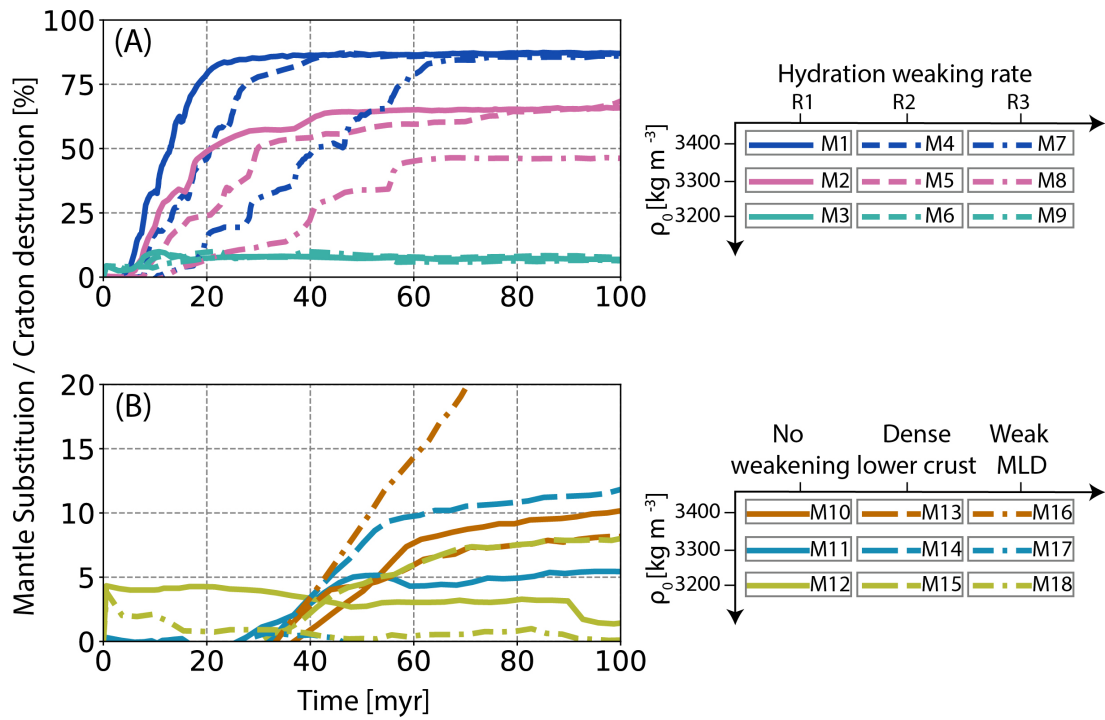


**Figure 4.** Temporal evolution of the substituted mantle percentage (equivalent to craton destruction) within the eastern block of the craton. Different lines representing different models are indexed beside each graph. Panel (A) shows models without hydration weakening, while panel (B) shows models with hydration weakening. Note the different scales of the Y-axes.

215 M4) and around 70% (models M2, M5) within approximately 20-40 Myr, respectively  
 216 (Fig. 4 A). Craton destruction is slower with R3 weakening rate. With a reference den-  
 217 sity of  $3400 \text{ kg m}^{-3}$  in model M7, only 50 % craton is destroyed within 40 Myr, and for  
 218 model M8 with reference density of  $3300 \text{ kg m}^{-3}$ , the destruction is only 25 % (Fig. 4  
 219 A).

### 220 3.3 Effect of flat slab, ecologitaton, and mid-lithospheric discontinuity

221 In the subsequent models (M10-M18), we explore the impact of top-to-bottom de-  
 222 struction mechanisms without incorporating hydration-induced weakening. Initially, we  
 223 focus solely on the influence of flat slab subduction without weakening the craton (mod-  
 224 els M10-M12). Despite the subducting slab causing significant mantle perturbation, the  
 225 craton remains unaffected. Even when the craton is significantly denser than the under-  
 226 lying mantle (model M10), stability is maintained as long as its viscosity exceeds  $10^{24}$   
 227 Pa s (Fig. S1). Tracking mantle substitution reveals minimal replacement of cratonic ma-  
 228 terial by new mantle, with the cratons remaining unaffected in all three models (M10-  
 229 M12) (Fig. 4 B, solid lines).

230 Introducing a denser lower crust theoretically allows for the development of crustal  
 231 drips capable of foundering through the underlying cratonic lithosphere and potentially  
 232 destroying it (Gao et al., 2004). We investigate this scenario by incorporating an inten-  
 233 tionally thick crust at a depth of 30 to 70 km, with densities reaching up to  $3500 \text{ kg m}^{-3}$   
 234 (models M13-M15, Table S2). Model M13 features the highest density lower crustal layer  
 235 ( $3500 \text{ kg m}^{-3}$ ). Despite the high density, lower crustal foundering is not observed in this  
 236 model (Fig. S2). Tracking mantle phases indicates that less than 10% of the mantle sub-  
 237 stitutes the densest cratonic material, with negligible material substitution in the other  
 238 two models with dense lower crust (Fig. 4 B, dashed lines). This suggests that the pres-  
 239 ence of the lower crust cannot lead to craton destruction in our models.

240 In another scenario, we examine the effect of the weak mid-lithospheric disconti-  
 241 nuity (MLD) (models M16-M18). The reference density ( $\rho_o$ ) of the weak MLD is set at  
 242  $3300 \text{ kg m}^{-3}$ , and wet olivine rheology is imposed to weaken it. Similarly, we vary the  
 243 craton's density in three models akin to previous models. In model M16, the craton's  
 244 reference density is kept at  $3400 \text{ kg m}^{-3}$  (Table S2). The mantle replacement curve shows  
 245 significant craton destruction for model M16. However, the craton delaminates beneath  
 246 the weak MLD from its western part, making it inconsistent with the geological obser-  
 247 vations (Fig. S3). Craton destruction remains negligible in models M17-M18 (Fig. 4 B,  
 248 dashdot lines).

## 249 4 Discussion

250 The destruction of the eastern part of the NCC has been widely acknowledged. Sev-  
 251 eral mechanisms are proposed to understand the reasons for the destruction (Gao et al.,  
 252 2004; J. Liu et al., 2019; Menzies et al., 1993; F.-Y. Wu et al., 2019; J. Zheng et al., 2005;  
 253 Zhu et al., 2012) including hydration weakening, crustal foundering, and decoupling due  
 254 to a weak MLD. It is crucial to emphasize that only the eastern-central part of the cra-  
 255 ton was subjected to destruction, while the western part remained intact. To determine  
 256 the most viable mechanism for the NCC's destruction, numerical models are developed  
 257 to simulate relevant geological scenarios.

258 Our results indicate that if cratons can be weakened rapidly (R1 or R2 weakening  
 259 rate), slightly faster than the diffusive timescale of water in the upper mantle (R3), 50-  
 260 80% of a craton can be destroyed within approximately 15-20 Myr, and 70-90% within  
 261 around 40 Myr. These findings are consistent with geological observations that suggested  
 262 rapid destruction of the NCC within 20-40 Myr (J. Liu et al., 2019; Chen et al., 2017).  
 263 Accelerated hydration weakening could be an effect of rapid reaction between carbon-

264 atite melt and pyroxene minerals of the cratonic lithosphere (X. Wang et al., 2022) that  
 265 can form potential pathways for water to diffuse through the craton. Previous studies  
 266 indicated higher water content in the Cretaceous lithospheric mantle of the eastern part  
 267 compared to the western counterpart (Xia, Liu, et al., 2013; Xia, Hao, et al., 2013). Be-  
 268 sides subduction zone fluids, substantial carbonate sediments may have been introduced  
 269 in this region (Chen et al., 2016; X. Wang et al., 2022), erupting as carbonatite magma  
 270 and accelerating hydration weakening within the NCC (X. Wang et al., 2022).

271 We have observed that densities higher than the underlying mantle ( $\sim 3200 \text{ kg m}^{-3}$ )  
 272 and viscosities of the order of  $10^{22} \text{ Pa s}$  are critical for the destruction of 70-90% of the  
 273 craton in our models (M1, M2, M4, M5, M7, M8). Failure to meet either of these condi-  
 274 tions does not lead to significant destruction (see Table S2). Even in the case where  
 275 a craton's density exceeds that of the underlying mantle, but the viscosity remains of  
 276 the order of  $10^{24} \text{ Pa s}$ , no lithospheric drips form (e.g., models M10, M13, M15). Con-  
 277 versely, when viscosity decreases below  $10^{22} \text{ Pa s}$  but the density does not surpass the  
 278 underlying mantle ( $\sim 3200 \text{ kg m}^{-3}$ ), the weakened craton remains intact in this short  
 279 time of 100 Myr (e.g., models M3, M6, M9). Therefore, craton destruction is profoundly  
 280 reliant on both parameters. The viscosity estimate aligns with previous studies indicat-  
 281 ing that cratons with viscosities of the order of  $10^{23}$  to  $10^{24} \text{ Pa s}$  can endure for at least  
 282 a few hundred million years (Paul et al., 2019; Paul & Ghosh, 2020).

283 For similar reasons, lower crustal foundering fails to destroy the craton in our mod-  
 284 els. Developing crustal instabilities through a highly viscous cratonic lithosphere, even  
 285 with a thick and dense lower crust, proves unfeasible. The foundering of the lower crustal  
 286 layer might be effective in active orogens like the Tibetan plateau (Houseman & Mol-  
 287 nar, 1997), where the mantle beneath the lower crust is sufficiently hot and weak to ini-  
 288 tiate such crustal instabilities. Hence, our models do not support the hypothesis of ex-  
 289 clusive lower crustal foundering leading to destruction.

290 Weak mid-lithospheric discontinuities (MLD) has also proven ineffective in the NCC  
 291 destruction in most instances, except when a denser craton is positioned beneath MLD  
 292 (model M16). In such scenarios, viscous decoupling becomes more efficient, promoting  
 293 the delamination of the dense cratonic root beneath the MLD. A similar type of craton  
 294 modification has been proposed for the African craton (Z. Wang et al., 2017). However,  
 295 due to the geometrical configuration, the eastern part of the North China Craton (NCC)  
 296 was shielded by a flat slab, and destruction initiated from the western margin in pres-  
 297 ence of a weak MLD. This scenario does not agree with the geological observations, chal-  
 298 lenging the viability of the MLD-induced hypothesis in this case. A previous study mod-  
 299 eled the destruction of the NCC using a weak MLD (Shi et al., 2020); however, they did  
 300 not consider the presence of a flat slab, which could have shielded the eastern block for  
 301 an extended period. Additionally, the status of 'weak' MLDs under cratons is highly de-  
 302 bated (Z. Wang & Kusky, 2019), and further studies are required to determine whether  
 303 a weak MLD even existed in this region during the Jurassic.

304 Based on all 18 models we suggest that hydration weakening and subse-  
 305 quent destruction is the most viable mechanism for the NCC destruction. We note that  
 306 hydration and subsequent weakening are not explicitly modeled in our investigation. In-  
 307 stead, we use a simplified approximation to mimic the timescales of water transport and  
 308 the effects of metasomatism, thus matching the potential of hydration weakening by first  
 309 order. Furthermore, 2D models do not allow us to rule out craton destruction by trench-  
 310 parallel motion. Our results do, however, suggest that material that is not dense enough  
 311 or too viscous cannot be recycled within the time frame assumed for the NCC.

## 5 Conclusions

Our results demonstrate that density and viscosity of the lower cratonic lithosphere both have to meet critical conditions to allow for destruction. Only if the craton's density is higher than that of the underlying mantle and its viscosity is lower than  $10^{22}$  Pa s, drips can form and sink into the mantle. Meeting these conditions, results in 70 - 90% destruction of the lower, eastern NCC. We find that top-to-bottom processes such as foundering due to a dense lower crust or delamination along a weak MLD fail to meet both critical conditions and result in a largely stable craton. In our models, only the bottom-to-top process of flat slab-induced hydration and subsequent weakening fulfills both conditions and is therefore the most viable explanation for the NCC destruction. To match the established destruction timescale of 20-40 Myr, the hydration of the eastern NCC needed to be sufficiently fast which was likely facilitated by subduction channel fluids and the abundant carbonatite melts.

## 6 Open Research

Numerical models were developed using the open source finite difference code LaMEM (<https://github.com/UniMainzGeo/LaMEM>). The model geometry is drawn using another open source MATLAB code geomIO (<https://bitbucket.org/geomio/geomio/src/master/>). The current version of geomIO used in this study can be downloaded from <https://zenodo.org/records/10878180>. Example LaMEM input file and geomIO files are uploaded in <https://zenodo.org/records/10886215> and <https://jyotirmoy.github.io/research/craton/>.

## Acknowledgments

AS received funding from the DFG grant TH 2076/8-1. AP received funding from the DFG grant TH 2076/7-1. JP thanks Dr. Mahesh Halder for presubmission review of this manuscript. Publication cost is funded by Open Access Publishing Fund of the University of Bayreuth.

## References

- Bauville, A., & Baumann, T. S. (2019). geomio: An open-source MATLAB toolbox to create the initial configuration of 2-d/3-d thermo-mechanical simulations from 2-d vector drawings. *Geochemistry, Geophysics, Geosystems*, *20*(3), 1665–1675.
- Chen, C., Liu, Y., Foley, S. F., Ducea, M. N., Geng, X., Zhang, W., ... Wang, Z. (2017). Carbonated sediment recycling and its contribution to lithospheric refertilization under the northern North China Craton. *Chemical Geology*, *466*, 641–653.
- Chen, C., Liu, Y., Foley, S. F., Ducea, M. N., He, D., Hu, Z., ... Zong, K. (2016). Paleo-Asian oceanic slab under the North China craton revealed by carbonatites derived from subducted limestones. *Geology*, *44*(12), 1039–1042.
- Conrad, C. P., & Lithgow-Bertelloni, C. (2006). Influence of continental roots and asthenosphere on plate-mantle coupling. *Geophysical Research Letters*, *33*(5).
- Conrad, C. P., & Molnar, P. (1999). Convective instability of a boundary layer with temperature- and strain-rate-dependent viscosity in terms of 'available buoyancy'. *Geophysical Journal International*, *139*(1), 51–68.
- Demouchy, S. (2010). Diffusion of hydrogen in olivine grain boundaries and implications for the survival of water-rich zones in the Earth's mantle. *Earth and Planetary Science Letters*, *295*(1-2), 305–313.
- Demouchy, S., Mackwell, S. J., & Kohlstedt, D. L. (2007). Influence of hydrogen on Fe–Mg interdiffusion in (Mg, Fe) O and implications for Earth's lower mantle. *Contributions to Mineralogy and Petrology*, *154*(3), 279–289.

- 360 Gao, S., Rudnick, R. L., Yuan, H.-L., Liu, X.-M., Liu, Y.-S., Xu, W.-L., ... Wang,  
361 Q.-H. (2004). Recycling lower continental crust in the North China craton.  
362 *Nature*, *432*(7019), 892–897.
- 363 Hammouda, T., & Laporte, D. (2000). Ultrafast mantle impregnation by carbonatite  
364 melts. *Geology*, *28*(3), 283–285.
- 365 Hirth, G., & Kohlstedt, D. (2003). Rheology of the upper mantle and the man-  
366 tle wedge: A view from the experimentalists. *Geophysical monograph-american*  
367 *geophysical union*, *138*, 83–106.
- 368 Houseman, G. A., & Molnar, P. (1997). Gravitational (Rayleigh–Taylor) instabil-  
369 ity of a layer with non-linear viscosity and convective thinning of continental  
370 lithosphere. *Geophysical Journal International*, *128*(1), 125–150.
- 371 Kohlstedt, D. L., & Mackwell, S. J. (1998). Diffusion of hydrogen and intrinsic point  
372 defects in olivine. *Zeitschrift für physikalische Chemie*, *207*(1-2), 147–162.
- 373 Liao, J., & Gerya, T. (2014). Influence of lithospheric mantle stratification on  
374 craton extension: Insight from two-dimensional thermo-mechanical modeling.  
375 *Tectonophysics*, *631*, 50–64.
- 376 Liu, J., Cai, R., Pearson, D. G., & Scott, J. M. (2019). Thinning and destruction  
377 of the lithospheric mantle root beneath the North China Craton: A review.  
378 *Earth-Science Reviews*, *196*, 102873.
- 379 Liu, L., Liu, L., Xu, Y.-G., Xia, B., Ma, Q., & Menzies, M. (2019). Development  
380 of a dense cratonic keel prior to the destruction of the North China Craton:  
381 Constraints from sedimentary records and numerical simulation. *Journal of*  
382 *Geophysical Research: Solid Earth*, *124*(12), 13192–13206.
- 383 Mei, S., & Kohlstedt, D. (2000). Influence of water on plastic deformation of olivine  
384 aggregates: 2. Dislocation creep regime. *Journal of Geophysical Research: Solid*  
385 *Earth*, *105*(B9), 21471–21481.
- 386 Menzies, M. A., Fan, W., & Zhang, M. (1993). Palaeozoic and cenozoic lithoprobes  
387 and the loss of > 120 km of Archaean lithosphere, Sino-Korean craton, China.  
388 *Geological Society, London, Special Publications*, *76*(1), 71–81.
- 389 Paul, J., & Ghosh, A. (2020). Evolution of cratons through the ages: A time-  
390 dependent study. *Earth and Planetary Science Letters*, *531*, 115962.
- 391 Paul, J., Ghosh, A., & Conrad, C. P. (2019). Traction and strain-rate at the base of  
392 the lithosphere: an insight into cratonic survival. *Geophysical Journal Interna-*  
393 *tional*, *217*(2), 1024–1033.
- 394 Pusok, A. E., & Stegman, D. R. (2020). The convergence history of India-Eurasia  
395 records multiple subduction dynamics processes. *Science Advances*, *6*(19),  
396 eaaz8681.
- 397 Riel, N., Duarte, J. C., Almeida, J., Kaus, B. J., Rosas, F., Rojas-Agramonte, Y., &  
398 Popov, A. (2023). Subduction initiation triggered the Caribbean large igneous  
399 province. *Nature Communications*, *14*(1), 786.
- 400 Ritsema, J., van Heijst, H. J., & Woodhouse, J. H. (2004). Global transition  
401 zone tomography. *Journal of Geophysical Research: Solid Earth*, *109*(B2),  
402 doi:10.1029/2003JB002610.
- 403 Shi, Y.-N., Niu, F., Li, Z.-H., & Huangfu, P. (2020). Craton destruction links to the  
404 interaction between subduction and mid-lithospheric discontinuity: Implica-  
405 tions for the eastern North China Craton. *Gondwana Research*, *83*, 49–62.
- 406 Spang, A., Baumann, T., & Kaus, B. J. (2022). Geodynamic modeling with un-  
407 certain initial geometries. *Geochemistry, Geophysics, Geosystems*, *23*(6),  
408 e2021GC010265.
- 409 Spang, A., Burton, M., Kaus, B. J., & Sigmundsson, F. (2022). Quantification of  
410 volcano deformation caused by volatile accumulation and release. *Geophysical*  
411 *Research Letters*, *49*(10), e2021GL097502.
- 412 Tang, J., Xu, W., Wang, F., & Ge, W. (2018). Subduction history of the Paleo-  
413 Pacific slab beneath Eurasian continent: Mesozoic-Paleogene magmatic records  
414 in Northeast Asia. *Science China Earth Sciences*, *61*, 527–559.

- 415 Tirel, C., Brun, J.-P., & Burov, E. (2008). Dynamics and structural development  
416 of metamorphic core complexes. *Journal of Geophysical Research: Solid Earth*,  
417 *113*(B4).
- 418 Wang, X., Zhang, J., Wang, C., Zong, K., & Xu, H. (2022). Experimental Con-  
419 straint on Ca-Rich Carbonatite Melt-Peridotite Interaction and Implications  
420 for Lithospheric Mantle Modification Beneath the North China Craton. *Jour-  
421 nal of Geophysical Research: Solid Earth*, *127*(9), e2022JB024769.
- 422 Wang, Z., & Kusky, T. M. (2019). The importance of a weak mid-lithospheric layer  
423 on the evolution of the cratonic lithosphere. *Earth-Science Reviews*, *190*, 557–  
424 569.
- 425 Wang, Z., Kusky, T. M., & Capitanio, F. A. (2017). Ancient continental lithosphere  
426 dislocated beneath ocean basins along the mid-lithosphere discontinuity: A  
427 hypothesis. *Geophysical Research Letters*, *44*(18), 9253–9260.
- 428 Wang, Z., Liu, L., Fu, Y., Zhao, L., Lin, J., Jin, Z., & Zheng, B. (2023). Multi-  
429 stage plate subduction controls intraplate volcanism and cratonic lithospheric  
430 thinning in Northeast Asia. *Earth-Science Reviews*, 104590.
- 431 Wu, F.-Y., Yang, J.-H., Xu, Y.-G., Wilde, S. A., & Walker, R. J. (2019). Destruction  
432 of the North China craton in the Mesozoic. *Annual Review of Earth and  
433 Planetary Sciences*, *47*, 173–195.
- 434 Wu, J. T.-J., Wu, J., & Okamoto, K. (2022). Intra-oceanic arc accretion along  
435 Northeast Asia during Early Cretaceous provides a plate tectonic context for  
436 North China craton destruction. *Earth-Science Reviews*, *226*, 103952.
- 437 Xia, Q., Hao, Y.-T., Liu, S.-C., Gu, X.-Y., & Feng, M. (2013). Water contents of  
438 the Cenozoic lithospheric mantle beneath the western part of the North China  
439 Craton: Peridotite xenolith constraints. *Gondwana Research*, *23*(1), 108–118.
- 440 Xia, Q., Liu, J., Liu, S.-C., Kovacs, I., Feng, M., & Dang, L. (2013). High water con-  
441 tent in Mesozoic primitive basalts of the North China Craton and implications  
442 on the destruction of cratonic mantle lithosphere. *Earth and Planetary Science  
443 Letters*, *361*, 85–97.
- 444 Xu, Y.-G. (2001). Thermo-tectonic destruction of the Archaean lithospheric keel  
445 beneath the Sino-Korean Craton in China: Evidence, timing and mechanism.  
446 *Physics and Chemistry of the Earth, Part A: Solid Earth and Geodesy*, *26*(9–  
447 10), 747–757.
- 448 Yang, J.-H., Wu, F.-Y., Wilde, S. A., Belousova, E., & Griffin, W. L. (2008). Meso-  
449 zoic decratonization of the North China block. *Geology*, *36*(6), 467–470.
- 450 Ye, Z., Fan, D., Tang, Q., Xu, J., Zhang, D., & Zhou, W. (2021). Constraining the  
451 density evolution during destruction of the lithospheric mantle in the eastern  
452 North China Craton. *Gondwana Research*, *91*, 18–30.
- 453 Zheng, J., Sun, M., Zhou, M.-F., & Robinson, P. (2005). Trace elemental and PGE  
454 geochemical constraints of Mesozoic and Cenozoic peridotitic xenoliths on  
455 lithospheric evolution of the North China Craton. *Geochimica et Cosmochim-  
456 ica Acta*, *69*(13), 3401–3418.
- 457 Zheng, Y., Xu, Z., Zhao, Z., & Dai, L. (2018). Mesozoic mafic magmatism in North  
458 China: Implications for thinning and destruction of cratonic lithosphere. *Sci-  
459 ence China Earth Sciences*, *61*, 353–385.
- 460 Zheng, Y.-F., Xiao, W.-J., & Zhao, G. (2013). Introduction to tectonics of China.  
461 *Gondwana Research*, *23*(4), 1189–1206.
- 462 Zhu, R.-X., Yang, J.-H., & Wu, F.-Y. (2012). Timing of destruction of the North  
463 China Craton. *Lithos*, *149*, 51–60.